Mapping of greenstone belts using aeromagnetic data in Eastern Dharwar Craton, India

M. Prasanthi Lakshmi*, S. Parveen Begum, A. Manglik and D. Seshu

Airborne Electromagnetics Division, CSIR-National Geophysical Research Institute, Hyderabad 500 007, India

The Eastern Dharwar Craton (EDC) in southern India comprises several thin, linear N–S and NW–SE trending greenstone belts that hold rich economic mineral deposits, surrounded by gneisses and granites of different ages. Very long, linear, high-frequency, high-amplitude magnetic anomalies trending along the E–W, NE–SW, ENE–WSW, NW–SE and N–S directions associated with several sets of dike swarms, fault shears and fractures forming a rhombic pattern over the granite-gneissic terrain in the western part of EDC hindered the recognition of these thin, linear belts. The N–S strike of the belts in the low-magnetic latitudes posed another limitation to demarcate these zones. A comprehensive relook into the regional aero-magnetic data using the prevailing interpretation techniques through diverse approaches helped identify the feeble magnetic signatures due to known narrow zones and enabled us to map hitherto unknown belts, namely Kurnool and Lattavaram–Atmakuru. 2.5D GM-SYS modelling has been carried out to delineate the vertical disposition of known belts that reaffirmed the existence of newly inferred belts. Isolated magnetic anomalies are also modelled for source-body parameters.

Keywords: Aeromagnetic data, greenstone belts, low-magnetic latitudes, magnetic anomalies.

INTERPRETATION of magnetic data at low magnetic latitudes is complex as the shape of the anomalies is controlled by several factors since the magnetic field is a vector field. The direction of magnetization depends on geomagnetic inclination of the area, strike of the body and presence of permanent magnetization acquired by the body apart from induced magnetization. The reduced to the pole (RTP) technique resolves the ambiguity to some extent when the source is magnetized only by induction, as the RTP process does not consider the remanent magnetization and hence fails to exactly locate the anomaly peak over the source[1]. Further, very large amplitude correction factors required to suppress the N–S noise that develops in the RTP process at low magnetic latitudes also eliminate a component of the anomaly due to the N–S feature[2]. To avoid these problems, the general practice is to convert total magnetic intensity (TMI) anamoly data at low magnetic latitudes to reduced-to-equator (RTE) transform. However, RTE also does not consider the remanance component, if present.

In addition to the above limitation, locating the N–S features is a difficult task, since the N–S trending sources produce low-amplitude magnetic anomalies at low magnetic latitudes, as the magnetization vector aligns along the strike (N–S). When the flight lines are aligned N–S, the chances of cutting along the N–S trending body become least depending on the line spacing chosen and width of the magnetic source.

Geology of the area

The Dharwar Craton in India has been subdivided into the Eastern Dharwar Craton (EDC) and the Western Dharwar Craton (WDC), which are separated by the N–S trending Closepet granite[3]. While the EDC is dominated by several narrow greenstone belts with prevalent bimodal volcanics and some komatiites, the WDC is dominated by wider schist belts associated with metabasalts along with komatiite–tholeiite association and minor bimodal volcanic rocks. The important lithological units that occur in the EDC are peninsular gneiss, granite, narrow N–S trending greenstone belts and Proterozoic sediments of the Cuddapah basin[4]. Schist belts, granite–gneisses, N–S-oriented younger granitoids and mafic dikes form the basement of the Cuddapah basin.

The greenstone granite terrain surrounding the Cuddapah basin is mostly composed of metamorphosed volcano-sedimentary sequences ranging in age from 3.4 to 2.7 Ga, and was often affected by plutonism related to batholith emplacement. These schist belts are important sites of economic ore deposits of iron and manganese, and several hydrothermal deposits. The major schist belts and some small-scale structures such as schistosity trend predominantly in the N–S and NNW–SSE directions[5]. These are (a) Sandur, (b) Ramagiri–Penakacharla–Hungund, (c) Hutti–Kolar–Kadiri, (d) Narayanpet–Gadwal–Veligallu and (e) Nellur–Khammam greenstone belts. The Sandur schist belt lies within the Closepet granite[6–8]. These greenstone belts are surrounded by younger granitoid

*For correspondence. (e-mail: prasu_mp@rediffmail.com)

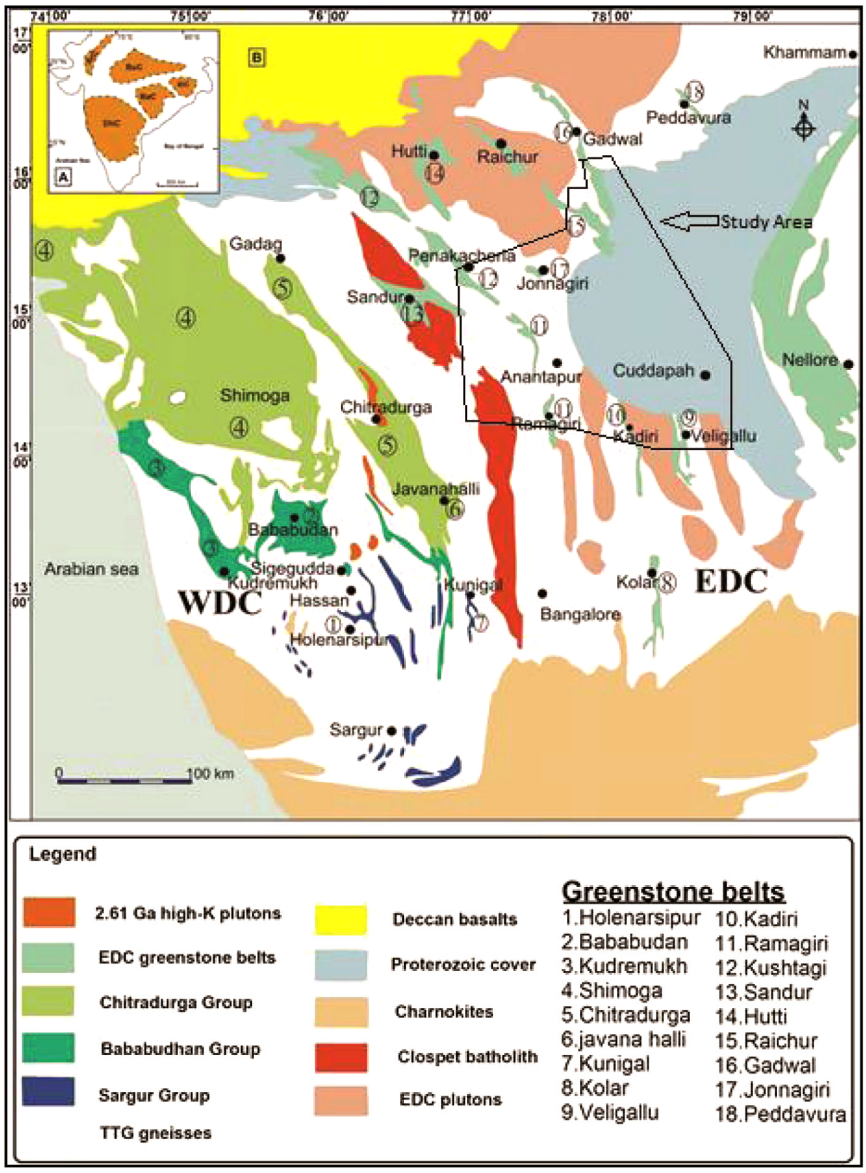

Figure 1. Generalized geological map of the Dharwar Craton, India (after refs 9, 10).

batholiths. Most of the Ramagiri–Penakacharla–Hungund belt and only parts of the Gadwal, Veligallu, Kadiri, Sundupalli and Sandur belts fall in the present study area. Several sets of dyke and fracture trends are marked along the E–W, NE–SW and NW–SE and N–S directions. The granite-gneissic terrain in the western part of the EDC comprises several kimberlitic provinces such as Wajrakarur, Narayanpet, Maddur and Kalyandurg, which are structurally controlled by a number of deep vertical faults and numerous sets of dykes. Figure 1 shows the generalized geological map of the Dharwar Craton[9,10].

Aeromagnetic data

Aeromagnetic data over the present study area were acquired by the National Geophysical Research Institute (NGRI), Hyderabad for the Geological Survey of India (GSI) during 1980–1982, as a part of the mineral exploration programme. These regional aeromagnetic surveys were flown along N–S lines with a line spacing of 1 km and mean terrain clearance of 150 m. Instead of digitizing the already available manually drawn contour maps to avoid manual bias, the aeromagnetic data available on drafted magnetic sheets (digitized from flight analogue records) were read and fed into the database. Figure 2 shows the TMI anomaly image created by gridding these data with a grid cell size of 200 m. High amplitudes are represented by pink to red colours, while deep blue colour represents the lowest amplitude.

This familiar aeromagnetic image characteristically differentiates the Cuddapah basin in the east and granite-gneissic terrain in the west. Typical smoothly varying

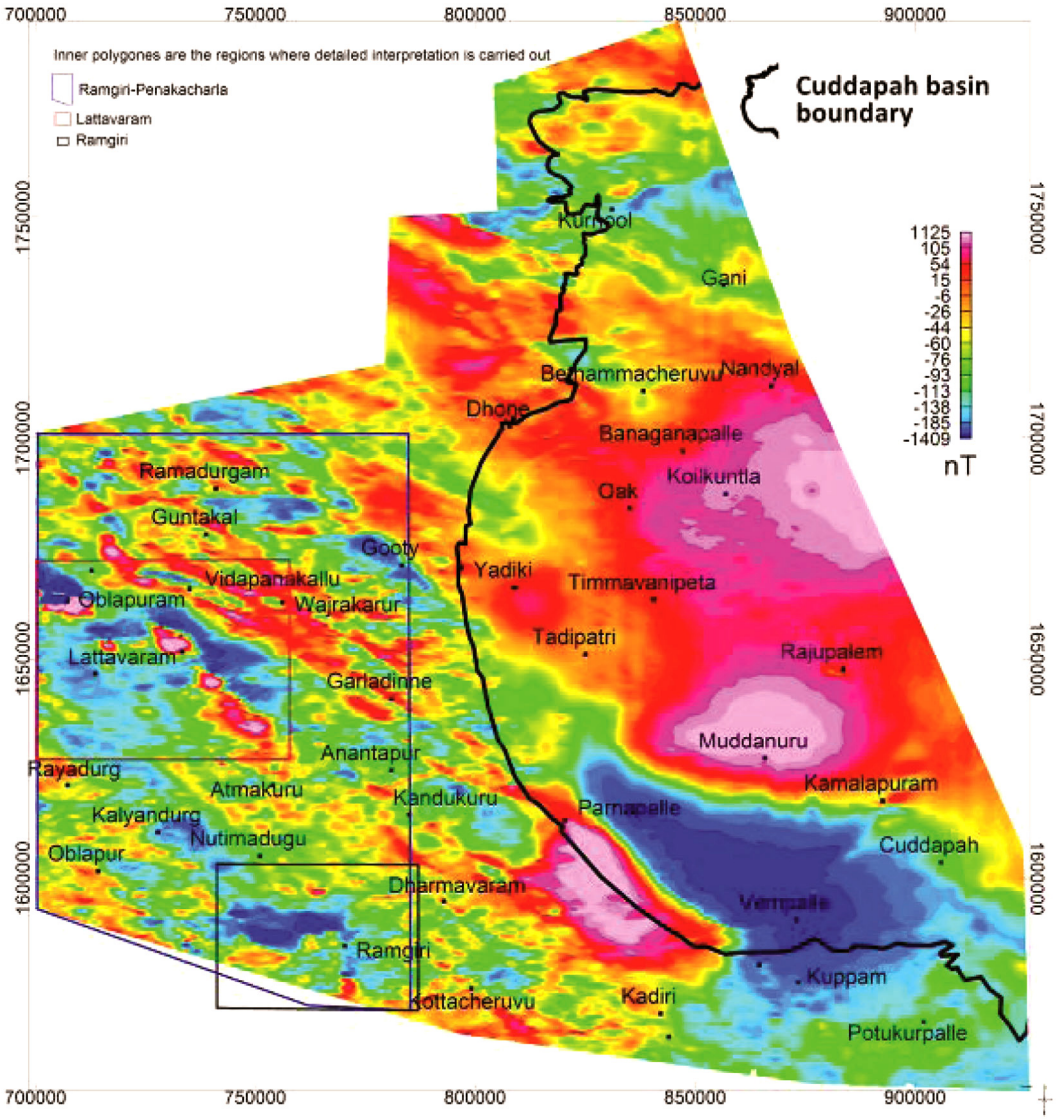

Figure 2. Total magnetic intensity anomaly image. (Areas where detailed analysis was done are shown in rectangles.)

long-wavelength anomalies of moderate intensity, with roughly E–W trends continuing from the west, define the Proterozoic sediments with a few high-frequency trends representing sills along and around the western margin of the basin. Numerous long, linearly extending high-frequency anomalies in the western part of the study area represent the granite-gneissic terrain. The anomaly patterns must be due to basement complexes and show that this area is intensely disturbed with innumerable number of dykes and fractures extended mostly in ENE–WSW and NW–SE, E–W and N–S directions.

With the limitations discussed earlier in the text, characteristic magnetic anomalies are seldom observed over the N–S trending schist belts which are narrow. Wider parts of the belts, especially when associated with mafic/ultramafic suits and/or banded iron formations (BIFs), produce high-amplitude magnetic anomalies at some places. One such case is over the NW–SE trending southeastern fringe of the Sandur schist belt. Some of the wider belts with anomalies of moderate amplitude and aligned in a general NW–SE trend of the Dharwar Craton, are not discriminable. Another case study of recognizing the extension of the schist belt is given in the northeastern corner of the Cuddapah basin[11]. In this region, mapping of the belt was successful owing to very high amplitude (of the order of 13,500 nT) magnetic anomalies produced by BIFs. Another case study on mapping the possible extension of the Kadiri schist belt into the Cuddapah basin utilized the sequential trend suppression in a few directions to enhance the trend of the belt[12]. There are several other studies available in the literature pertaining to mapping and estimating the depth and thickness of BIFs[13–15]. In this study we map the possible extents of the known greenstone belts and analyse the

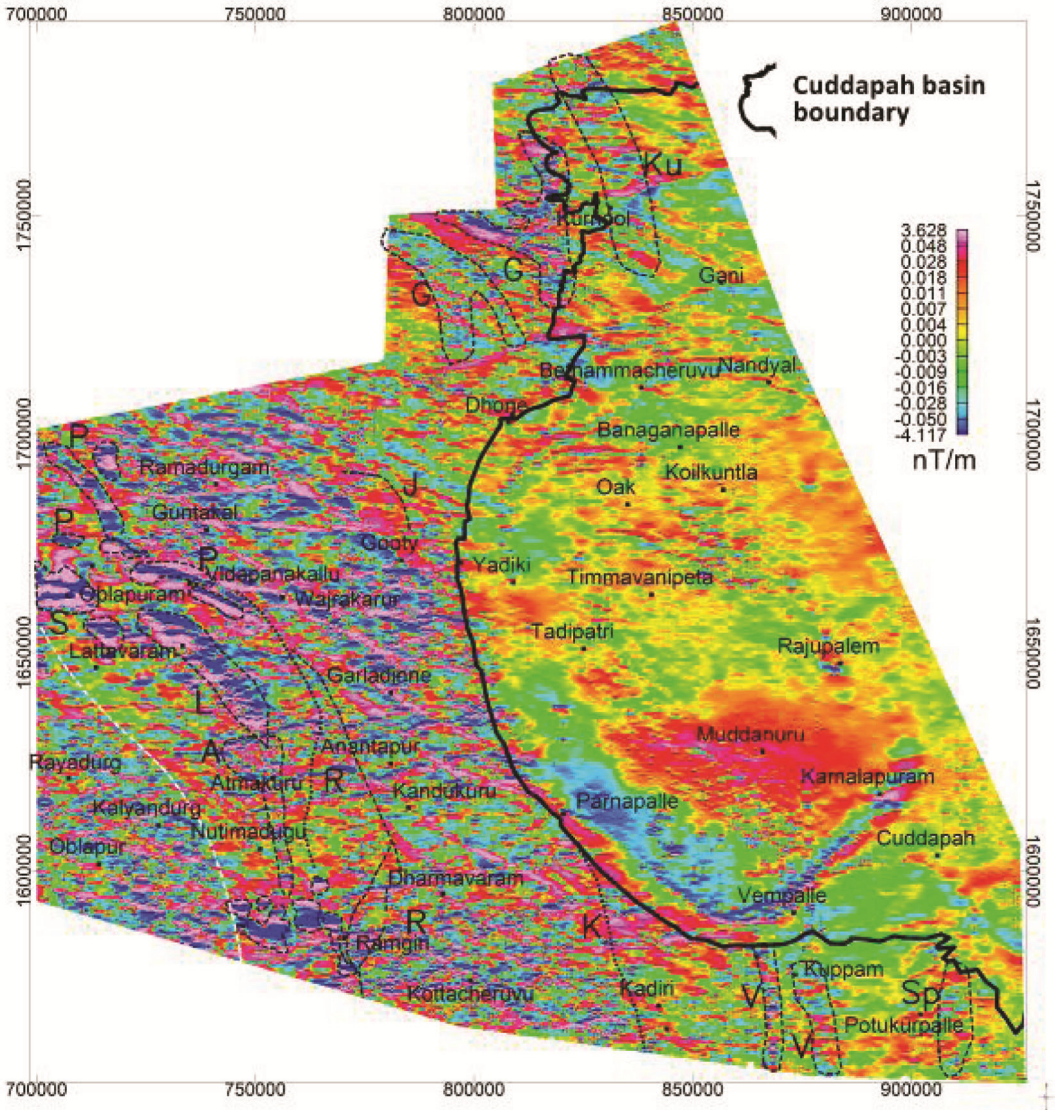

Figure 3. First vertical derivative of RTE image. Inferred boundaries of the schist belts are marked with black dashed lines. Known schist belts: G, Gadwal; J, Jonnagiri; K, Kadiri; P, Penakacherla; R, Ramagiri; S, Sandur; Sp, Sundupalli and V, Veligallu. Newly inferred belts: Ku, Kurnool; A, Atmakuru and L, Lattavaram. White dashed line is the inferred contact of Closepet granite with the EDC.

area using available old and regional aeromagnetic data with a new perspective.

Methodology

The N–S trending features are neither perfectly uniformly magnetized nor exhibit a perfect N–S strike in real geological conditions. Faulting, folding, deformations[16], non-uniform distribution of magnetite mineral content, variations in thickness along the strike and several other factors aid in creating feeble anomalies aligned N–S (obliterating the ideal conditions of non-detectability of the N–S features). The aim here is to enhance these weak anomalies to identify the associated geological structure.

There are several techniques available in the literature, such as vertical derivative and analytical signal (total gradient) which enhance the anomalies. The first vertical derivative of TMI is computed to enhance the anomalies due to shallower magnetic sources for a better insight into the near-surface structures. The analytical signal technique, which uses gradients of the total magnetic field in three orthogonal directions, is proved to be dependent only on the depth and independent of the directions of magnetization[17–19] (of both induced and remanant, the analytical signal is independent of remanence). The peaks of the anomaly closures in the analytical signal maps generally indicate the edges of the sources[20]. A detailed quantitative analysis on the use of 2D and 3D analytical signal approaches over the prism

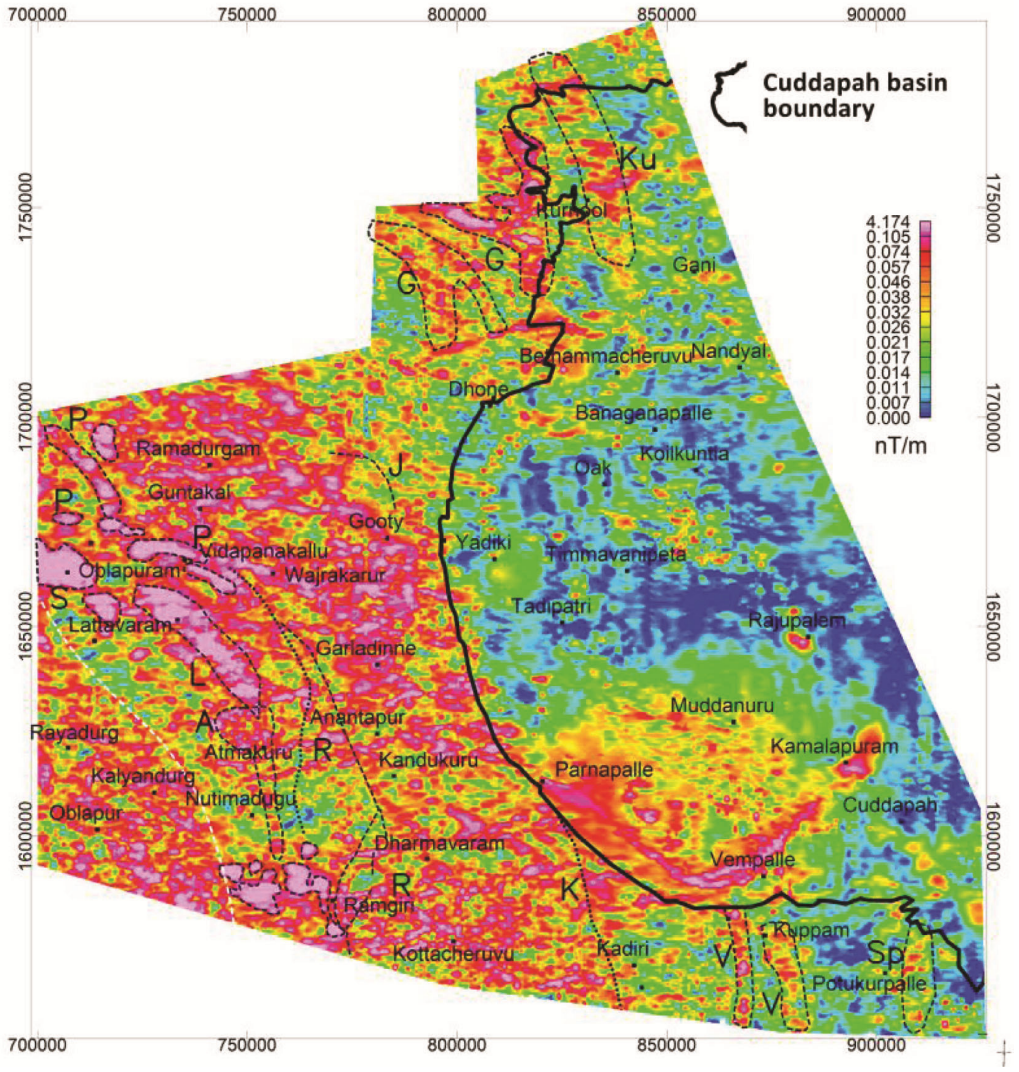

Figure 4. Analytical signal image (index followed from Figure 3).

and sheet model and calculation of depth to the magnetic sources is given in MacLeod *et al.*[21]. Figures 3 and 4 show the first vertical derivative of RTE of TMI (VDRTE) and analytical signal image respectively.

We basically examined schist belts in the study area according to their width, N–S linearity and amplitude of anomalies associated with the belts due to sources like BIFs and other ultramafics. Thin N–S trending belts/parts of the belts were identified and mapped based on the frequency and alignment of the anomalies. Broad and intense anomalous zones were identified based on the characteristics of the known belts in the surroundings. These intense anomalous zones were modelled in 1D (MAGMOD) and 2.5D (GM-SYS) to determine the depths.

MAGMOD is a software[22], used to calculate source parameters (size and shape) of discrete anomalies[22]. The user provides a field profile and selects one of the several available geometric models as a possible geological source. Starting values of various parameters of the model body provided by the user are employed in the computation of theoretical anomaly profile for that body, which is then compared by a least-squares method with the field profile. The method of Marquardt[23] is then used to adjust the body parameters so that subsequent iterations converge as rapidly as possible to give the body parameters which would best account for the observed anomaly. The function to be minimized is the weighted sum of squared deviations between the observed magnetic anomaly and calculated anomaly at the data points. In the case of the PRISM model, the function to be minimized is

$$S = \sum_i W_i \{T_i - (T_0 + AX_i + BY_i) - f(X_i, Y_i, X_0, Y_0; M, d, h, t, X, Y; I, D, \varphi, \tau)\}^2, \quad (1)$$

where T_i is the observed magnetic anomaly (total field or vertical field) at the point (x_i, y_i); T_0 is the regional background level for T at (0, 0); A, B are the X and Y component

respectively, of the slope of the regional background in the anomaly neighbourhood; f is the theoretical magnetic anomaly value (total field, vertical field or vertical gradient) of the interpretation model (which in this instance is PRISM); X_0, Y_0 are the X and Y coordinates respectively, of the centre point of the upper horizontal surface of PRISM and W_i is the weight that is assigned to the observation at (X_i, Y_i). For a 2D body, the parameters B, Y_0, Y and t are excluded, and f is independent of Y.

2.5D modelling is carried out using the GM-SYS package[24], an interactive computer programming software, in which magnetic response is computed based on the algorithms of Talwani and co-workers[25,26], and Won and Bevis[27] using an infinitely long prismatic body. Later, Shuey and Pasqulue[28] developed 2.5D profile modelling with a finite strike length using 2D algorithm of Cady[29,30].

Results and discussions

Mapping of Penakacherla schist belt

The Ramgiri–Hungund schist belt is divided into three parts: the Hungund schist belt in the northernmost part (outside the present study area), the Penakacharla schist belt in the central part and the Ramagiri schist belt in the southern part. The Penakacharla schist belt extends over a length of 110 km from north of Ramagiri till the southwestern corner of the study area. Pillow basalts are the abundant litho-units in this belt, while the other minor units are felsic volcanics, BIFs, cherts and carbonaceous shales. All the units are tightly folded and metamorphosed[8,31]. Special emphasis is given to this belt as it extends over a great length within the study area. A subset of TMI image covering this belt is shown in Figure 5 to highlight the amplitude range of the anomalies. To have a clear perception of the narrow geological features, a subset of the geological map of the study area is also considered (Figure 6) to show the depth estimates obtained from modelling. Vertical derivative of RTE (Figure 7) is utilized to enhance the anomalies of interest.

Throughout the length of the Penakacharla schist belt, only the NW to WNW trending wider curvilinear part (around Vidapanakallu, denoted by 'P' in Figure 5) manifests the TMI anomalies of higher amplitude ranging from 200 to 600 nT, with a high towards south and a low towards north. These WNW tending curvilinear bipolar anomalies form a zone and have a sharp contact with the granite-gneissic terrain towards north. These anomalies can be attributed to the meta-basalts and other mafic suites within the belt. They are differentiated from the other linear trending anomalies due to mafic dykes and shears in this region by their curvilinear nature, and the belt is demarcated based on analytical signal image (Figure 8).

The NNW trending segment of the belt in the northwestern corner of the study area (west of Ramadurgam) is again mapped based on the anomaly trends and analytical signal amplitudes. The remaining part of the belt to the south could not be marked continuously based on the anomaly amplitudes, as this part of the belt is narrow. Rather, it is marked following a break in the linear magnetic anomalies due to dykes and other basement trends (shown as dotted lines in Figures 5, 7 and 8).

Lattavaram–Atmakuru schist belt

Several high-amplitude bipolar anomalies around Lattavaram are found to form a zone (denoted by 'L' in Figure 5) extending WNW–ESE and parallel to the broader arm of the Penakacharla belt. Generally, the linear magnetic anomalies over the exposed basement complexes manifest the structural fabric like fault/fracture pattern, shear zones, mafic dykes, etc. Anomalies of variable amplitudes are expected based on the associated mafic content. Some NE–ENE faults have been found to offset this anomalous zone. These faults are shown in Figures 5, 7 and 8 as white dashed lines.

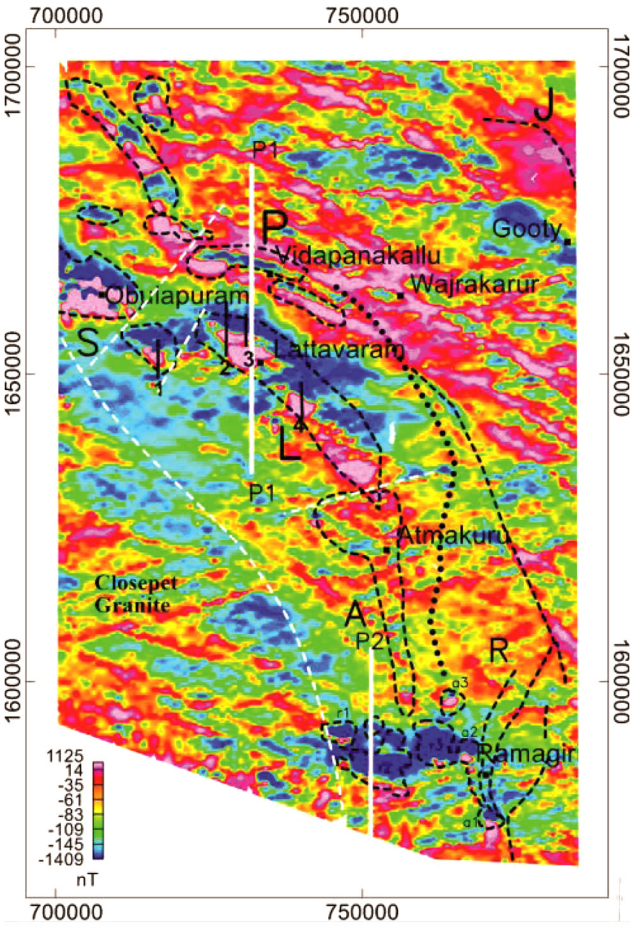

Figure 5. TMI image over a part of granite-gneissic terrain, west of the Cuddapah basin (index followed from Figure 3).

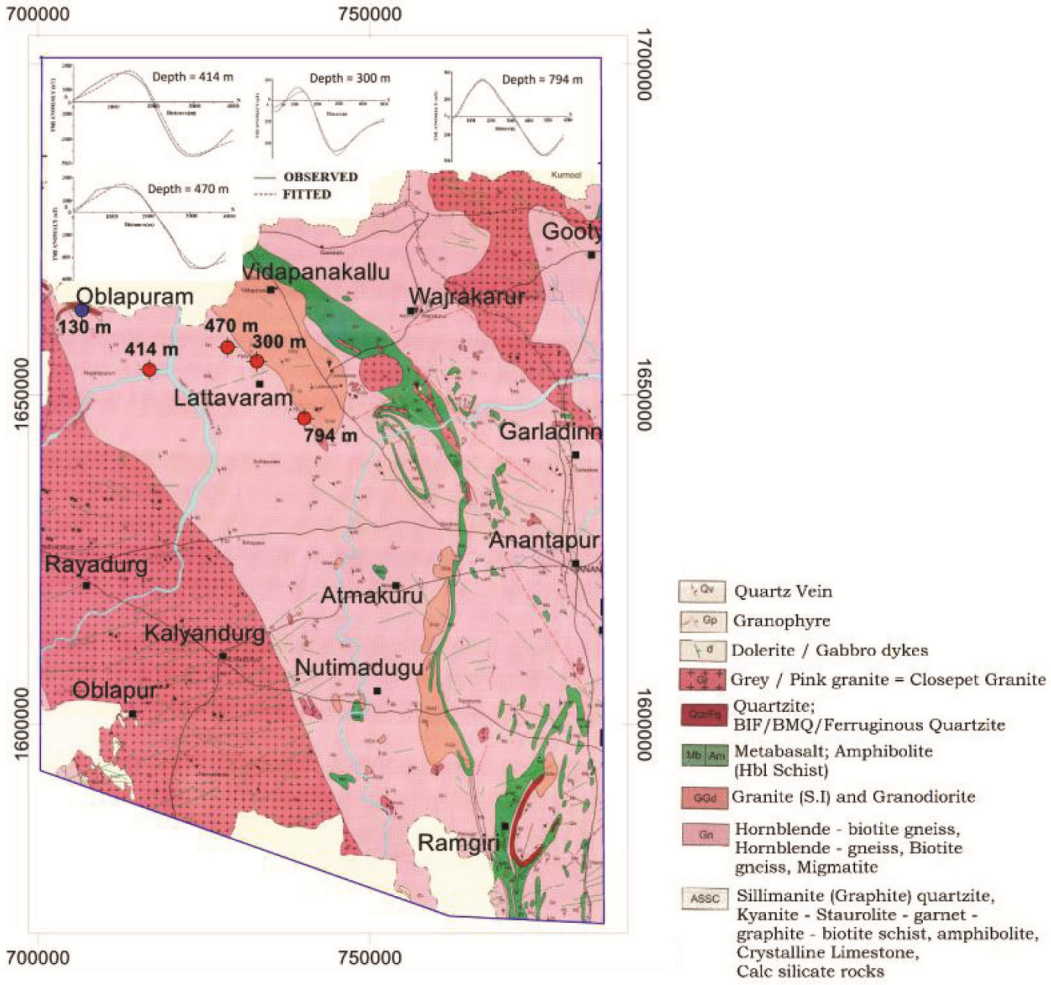

Figure 6. Detailed geological map over a part of the granite-gneissic terrain, west of the Cuddapah basin. (Red dots represent depths to the top of the magnetic sources). (Inset) Observed and fitted anomalies of the sources.

The individual anomalies are striking WNW–ESE (in zone L) consistently throughout the zone, with a high towards south and a low towards north. The zone is aligned NW–SE over a length of approximately 45 km and with anomaly widths around 5 km. The individual anomalies extend over a length of 5–7 km, with amplitude ranging from 2000 to 600 nT and gradually decreasing from NW to SE.

This zone (L) starts just east of the southeastern extreme of the Sandur schist belt with an offset by a NE–SW trending fault (marked as white dashed line between Obulapuram and Vidapanakallu in Figure 5). The shape of the TMI anomaly over this part of the belt is also similar to that over the Sandur schist belt, with a high towards the south and a low towards the north and with individual anomalies striking WNW–ESE (in zone L)[14]. Highly intense aeromagnetic anomalies (5000 nT) are noticed over the southeastern fringe of the Sandur schist belt. The ferruginous cherts, metabasalts, metagabbros and BIFs associated with this schist belt are interpreted to be the sources responsible for high-intensity magnetic anomalies.

This zone (L) is located over the region which is otherwise mapped as granite-gneissic terrain (Figure 6). The smoothly varying moderate-amplitude anomalies surrounding this zone represent the granite-gneissic basement complex. Magnetic anomalies of the order of only a few tens of nanotesla are shown up over the remaining part of the basement outcropping south and southeast of this zone. So, it can be inferred that either the basement complex over this zone is different from the marked geology, or the sources for these magnetic anomalies are at greater depths. The same characteristic anomaly shapes (of the newly mapped zone L), as those of BIFs of the Sandur schist belt, may suggest the possible extension of Sandur schist belt further southeast. Four such anomalies (marked with black lines 1–4 in Figure 5) are modelled using MAGMOD. The inset in Figure 6 shows the best-fitted anomaly along with the observed anomalies. Table 1 gives the fitted parameters of the source bodies for these four anomalies. Rao *et al.*[14] inferred the depth to the source from the Sandur schist belt in the west (marked with a blue dot in Figure 6) as 130 m. It is noteworthy

that the depth to the top of the causative sources in the newly inferred zone (marked with red dots in Figure 6) increases from NW to SE, which is indicative of continuation of the BIFs over the newly identified zone.

The most important observation is that this belt encompasses the western boundary of the NW trending granodiorite body, while the northern part of the Penakacherla schist belt encompasses the eastern fringe of the said granodiorite body. The sources of these intense anomalies must be due to mafic/ultramafic bodies forming a zone which might not have been exposed, or the continued belt of BIFs belonging to Sandur schist belt which are at some depth. Generally, intrusion of granites into the folded schist belts widens them. Two belts are separated by granitoid intrusion. From this point of view, it can be inferred that the interpreted intense anomaly zones encompassing the western side of the granitoid body belong to the Penakacherla belt.

Another N–S trending belt of high-frequency anomalies has been found as a continuation of the Lattavaram anomalous zone to its south through Atmakuru (Figure 7). This belt runs over a length of 35 km almost till the west of Ramagiri belt through Atmakuru. This zone is known as the Atmakuru belt.

2.5D Modelling of aeromagnetic data over the Lattavaram–Atmakuru belt

2.5D modelling has been carried out over a profile marked as P1 using GM-SYS package, in which the magnetic response is calculated based on the methods of Talwani and co-workers[25,26]. The magnetic profile P1 (Figure 5) runs over the Archaean basement complex, the intense anomalous zone marked as the Lattavaram–Atmakuru belt in the south, granodiorites in the central part and NW–SE trending part of the Penakacherla schist belt in the north. It extends in the S–N direction over a length of 35 km to the west of Lattavaram and Vidapanakallu, and has anomalies of various amplitudes. The conspicuous bipolar anomaly over the Lattavaram–Atmakuru belt is large both in amplitude and width than the anomalies over the known Penakacherla schist belt in the north.

The susceptibility values used for modelling were adopted from the literature[32–34]. Various susceptibility values assigned in the modelling are 0.013, 0.018, 0.0016,

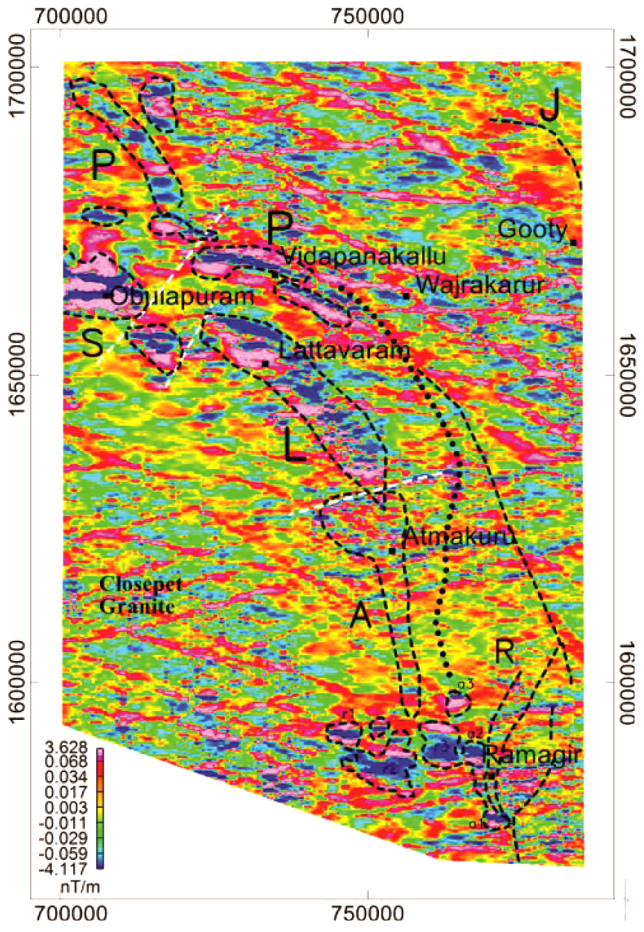

Figure 7. Vertical derivative of TMI image over a part of the granite-gneissic terrain, west of the Cuddapah basin (index followed from Figure 3).

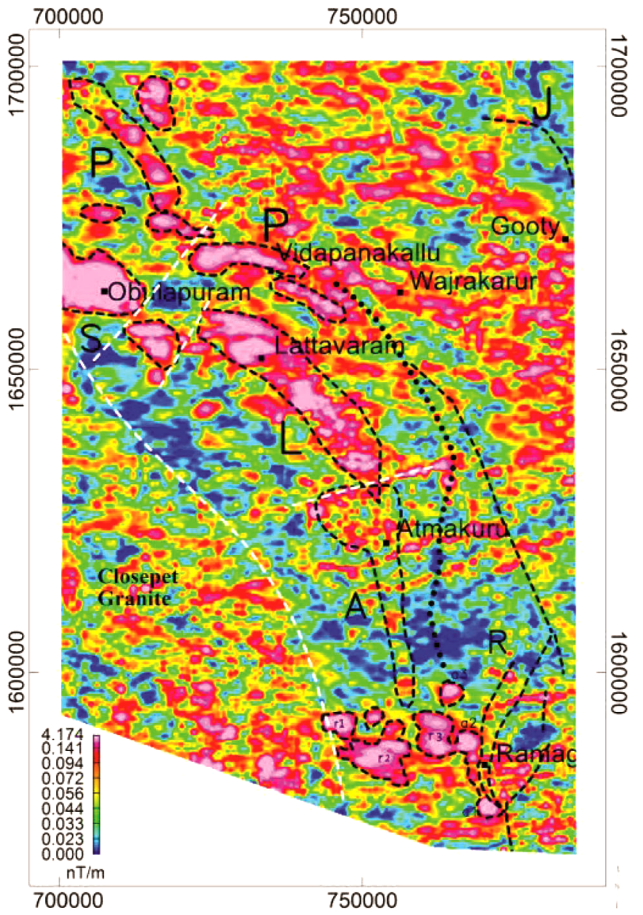

Figure 8. Analytical signal image over a part of the granite-gneissic terrain, west of the Cuddapah basin (index followed from Figure 3).

Table 1. Source parameters obtained from MAGMOD modelling

Body parameters	Results of Rao *et al.*[14]	Anomaly-1	Anomaly-2	Anomaly-3	Anomaly-4
Depth (m)	130	414	470	300	794
Half width (m)	350	600	860	684	1673
Dip (°)	65	80	80	74	45
Susceptibility (CGS units)	0.0367	0.0048	0.0044	0.0035	0.0099

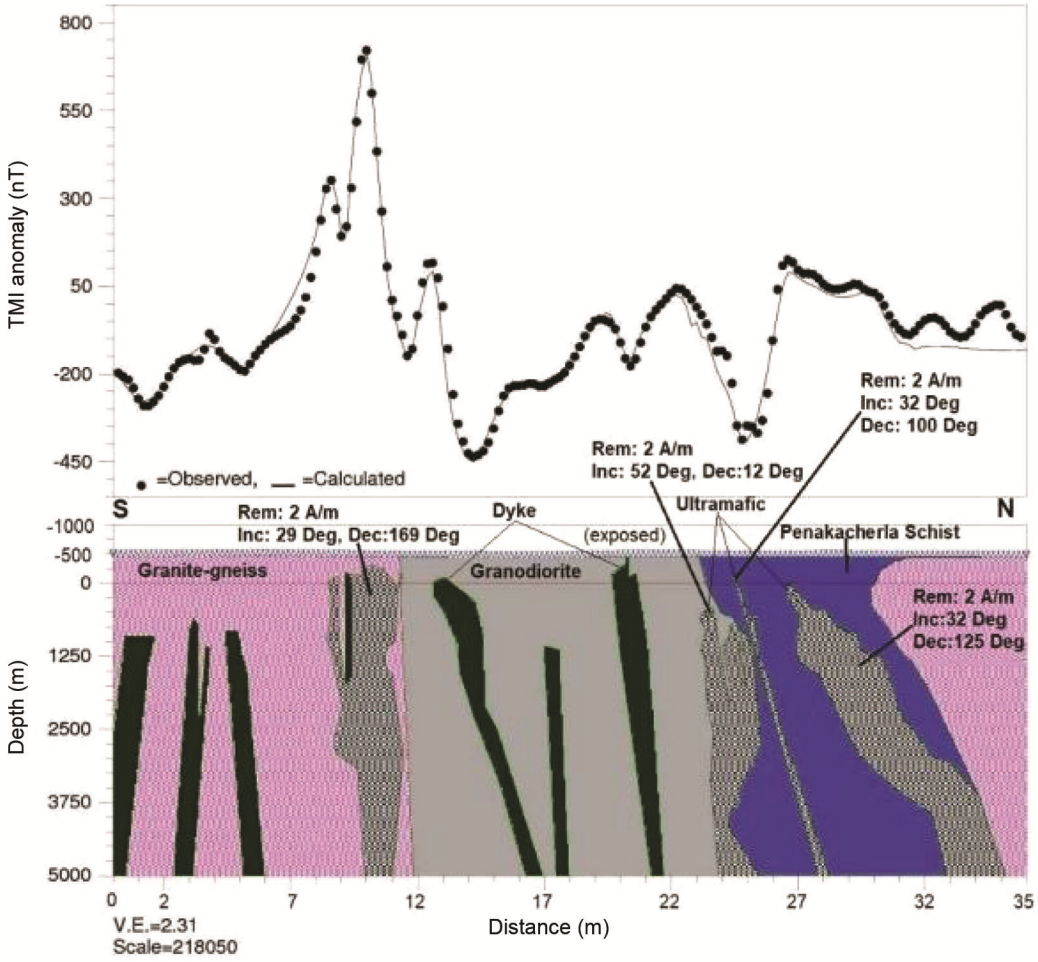

Figure 9. Modelling of the magnetic profile P1 using GM-SYS.

0.05 and 0.03 SI units for granite–gneiss, granodiorites, schists, mafics and dykes respectively. Remanence component values incorporated for mafic bodies are indicated in the model.

Modelling (GM-SYS) of the magnetic profile delineated gneiss, granodiorite and the Penakacherla schist belt with a number of (vertical/sub-vertical) subsurface dykes and ultra-mafics (Figure 9). The occurrence of ultramafic bodies in the profile P1 to the south of the Penakacherla belt affirms our inference/mapping of the existence of schist belt margining granodiorite towards north. The average depth to the top of the inferred ultramafic bodies in the Penakacherla belt is approximately 800 m and width is about 2 km. The depth to the top of the ultramafics in this profile on the inferred Lattavaram belt is approximately 300 m (and is in best correlation with point depth obtained from MAGMOD modelling). The average depth to the bottom of the bodies is ~5 km (depth to the bottom of the schist belts in the study area is reported as around 8 km in the published literature[14]).

Mapping of Ramagiri schist belt

The Ramagiri schist belt is one of the gold-bearing belts of the EDC[35,36]. It extends over a length of 50 km as three arms, namely eastern, central and western; the central arm is wider extending in the NNE direction. The eastern arm is thin and also extends in the NNE direction. Sheared metagabbros, chlorite schists, phyllites, ferruginous

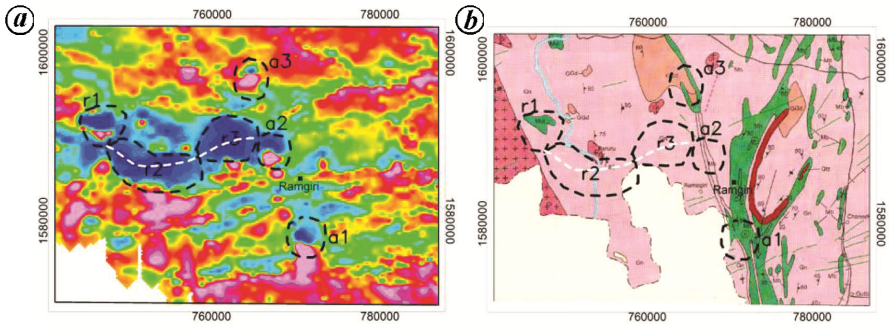

Figure 10. ***a***, TMI image over a part of the Ramagiri schist belt. (Circles indicate bipolar anomalies of amplitude more than 1000 nT.) ***b***, Geological map over a part of the Ramagiri schist belt (index for geological units followed from Figure 6).

quartzites and greenstones form the schist belt. Several granitoids also are associated with the Ramagiri greenstone belt.

Figure 10 *a* and *b* shows the TMI anomaly map and geological map covering this zone (R) respectively, at a smaller scale. The eastern and western arms of the schist belt can be delineated based on the breaks in anomaly trends. Though the central arm is wider, no prominent magnetic anomalies are found.

An isolated circular, bipolar anomaly (denoted by 'a1' in Figure 10 *a*) of the order of 1000 nT is noticed just south of the region where the three arms join together. Ghosh *et al.*[35] reported the occurrence of an ultramafic body at the southern end of the schist belt, which is outside of the study area. We infer that the bipolar anomaly identified (a1) over this part of the belt is also due to an ultramafic body. There are two more anomalies (a2 and a3 in Figure 10 *a*) of amplitude 1400 and 800 nT respectively, forming a north–south trending zone along the gap region between the Ramagiri and Penakacharla schist belts. This can be treated as the zone of greenstone remnants. This belt is marked as shear in the geological map (Figure 10 *b*). Based on these observations, this zone is inferred as a continuation of the Ramagiri belt of subdued nature.

Another anomaly (r1) with amplitude 1000 nT (with similar characteristics of a1–a3 anomalies) is observed over the lithological unit mapped as meta-ultramafic body in the geological map (Figure 10 *b*). The presence of exposed ultramafic unit and associated anomaly directed us to study the surrounding region. A series of elongated anomalies of bipolar nature with a high towards the south and a broad low towards the north are observed over the region (marked as 'r2' and 'r3' in Figure 10 *a*). These form a zone and join the N–S trending western arm of the Ramagiri belt. It can be inferred from these observations that this approximately east–west trending, arcuate-shaped zone is another arm representing the greenstone remnants of the Ramagiri schist belt. Presumably, only the lower 'Ultramafic Group' is left behind in this zone, while the middle 'Greenstone Group' and the upper 'Meta-Sedimentary Group' are absent/eroded.

The TMI profile P2 (Figure 5) is taken over the high-amplitude zone, west of the Ramagiri schist belt. This profile runs over a length of 28 km in south–north direction, cutting across the Closepet granite, peninsular gneiss and the exposed metagabbro. An amplitude of about 1000 nT is observed over this anomaly (r1 in Figure10 *a*). The model infers vertical dips of the exposed meta-ultramafic body (Figure 11). The other marked circular bipolar anomalies forming the belt may also indicate disposition of the subsurface meta-ultramafic bodies.

Mapping of Gadwal schist belt

The Gadwal schist belt lies outside the northwestern part of the Cuddapah basin and extends in two arms. One arm is just adjoining the basin boundary in the NNW–NS direction and the other arm extends in the NW–SE direction, with width varying between 1 and 10 km. Meta-basalts and felsic volcanics are the major litho-units that hold gold mineralization in this belt.

Large-amplitude TMI anomalies more than of 500 nT striking in the NW–SE direction are observed over the NW trending arms of the belt. The N–S oriented arm is devoid of such high-intensity TMI anomalies, but is characterized by several high–low pairs of moderate-magnitude anomalies, with a lateral extent limited to the width of the zone over its length. These are more prominently seen in VDRTE image (Figure 3). Both the zones are noted as 'G' in Figures 3 and 4. Probable extension of this belt beneath the Cuddapah basin at 2 km depth has been inferred from spectral analysis of the magnetic anomalies[13].

Kurnool schist belt

A band of high-frequency anomalies confined to a NNW striking zone is observed in Figure 3, within the Cuddapah basin to the east of the Gadwal schist belt. Anomaly characteristics are similar to the Gadwal schist belt, but with reduced amplitudes. Lower amplitude levels are attributed to the sediment cover/deeper nature of the sources. This zone is inferred as the Kurnool (Ku) schist belt and denoted as 'Ku' in Figures 3 and 4.

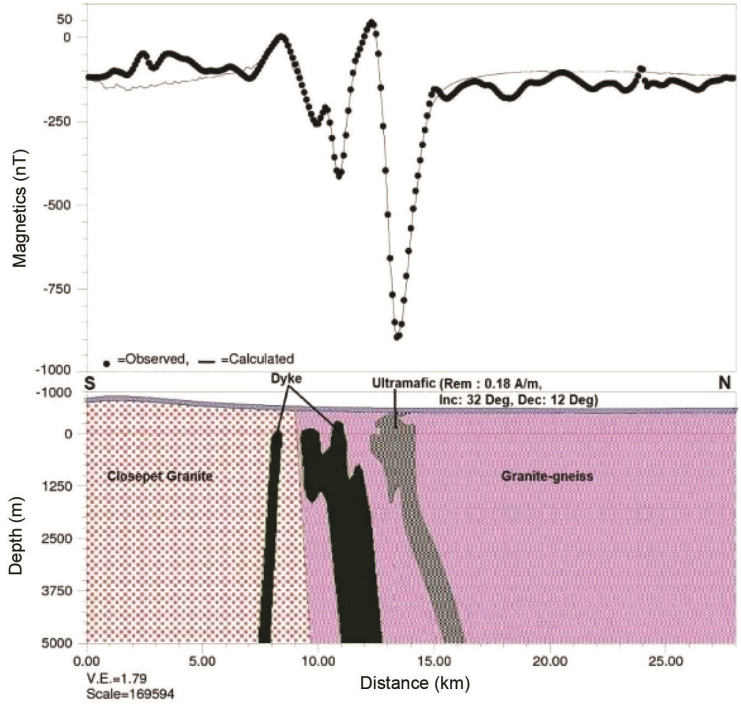

Figure 11. Modelling of the magnetic profile P2 using GM-SYS.

Mapping of Kadiri, Veligallu and Sundupalli schist belts

Three north–south trending zones comprising a series of alternating high–low anomalies of larger amplitude disturbing the regional basement trends are identified from the vertical derivative of RTE image (Figure 3) to the south of the Cuddapah basin. These are found to be associated with the two arms of the Veligallu schist belt and Sundupalli schist belt. They are demarcated as zones namely V and Sp respectively, in Figures 3 and 4. These belts are unambiguously mapped as they are surrounded by granitic plutons, which are manifested by comparatively smoothly varying magnetic field. A part of the Kadiri schist belt that exists to the west of the Veligallu belt, could not provide such anomalies perhaps due to the absence of mafic units within the belt. However, it is identified based on the break in the basement trends and other linear anomalies of east–west trending mafic dykes in this region. The probable extension of these schist belts into the basin is not noticed from the VDRTE image, due to the deeper nature of the anomalies that are not enhanced in vertical derivative technique.

Conclusion

Several N–S to NW–SE trending, thin, linear greenstone belts surrounding the Cuddapah basin give rise to TMI anomalies of various amplitudes and characteristics due to their orientation, width and association with metabasic/mafic-ultramafic units. Smaller and thin, north–south trending belts (Veligallu and Sundupalli) to the south of the Cuddapah basin are isolated based on their frequency characteristics. The amplitudes of anomalies are moderately high over the Gadwal schist belt and help identify the probable extent of this belt. A NNW–SSE trending belt to the east of the Gadwal belt with similar characteristic anomalies, is inferred to be extending beneath the Cuddapah sediments and is known as the Kurnool schist belt. The WNW–ESE trending zone comprising several high-amplitude anomalies (ranging from 800 to 2000 nT) of bipolar nature seems to be an extension of the Sandur schist belt, and is named as the Lattavaram–Atmakuru schist belt. 2.5D modelling of the aeromagnetic data delineated the newly inferred Lattavaram and known Penakacherla belts encompassing either sides of the granodioritic intrusion. Circular bipolar anomalies (more than 100 nT) over the N–S trending western arm of the Ramagiri schist belt are inferred to be due to metagabbros. This inference in turn helped identify extension of the western arm with meta-ultramafic units of greenstone remnants.

1. Grant, F. S. and Dodds, J., MAGMAP FFT processing system development notes. Paterson Grant and Watson Limited, 1972.
2. Mendonca, C. A. and Silva, J. B. C., A stable truncated series approximation of the reduction to the pole operator. *Geophysics*, 1993, **58**, 1084–1090.
3. Naqvi, S. M. and Rogers, J. J. W., *Precambrian Geology of India*, Oxford Monographs on Geology and Geophysics, Oxford University Press Oxford, 1987, p. 223.
4. Drury, S. A., A proterozoic intra-cratonic basin, dyke swarms and thermal evolution in South India. *J. Geol. Soc. India*, 1984, **25**, 437–444.

5. Mukhopadhyay, D., Structural pattern in the Dharwar craton. *J. Geol*., 1986, **94**, 167–186.
6. Sreeramachandra Rao, K., Regional surveys and exploration for gold in the granite–greenstone terranes of Andhra Pradesh. *Spec. Publ. Geol. Surv. India*, 2001, **58**, 11–27.
7. Manikyamba, C. and Khanna, T. C., Crustal growth processes as illustrated by the Neoarchean intraoceanic magmatism from Gadwal greenstone belt, Eastern Dharwar Craton, India. *Gondwana Res*., 2007, **11**, 476–491.
8. Manikyamba, C. and Kerrich, R., Geochemistry of alkaline basalts and associated high-Mg basalts from the 2.7 Ga Penakacherla Terrane, Dharwar Craton, India: an Archean depleted mantle-OIB array. *Precambrian Res*., 2011, **188**, 104–122.
9. Dominique, C., Jayananda, M., Chetty, T. R. K. and Peucat, J. J., Precambrian continental strain and shear zone patterns: South Indian case. *J. Geophys. Res.*, 2008, **113**, B08402; http://dx.doi.org/10.1029/2007JB005299.
10. Jayananda, M., Peucat, J., Chardonc, D., Krishna Raod, B., Fanninge, C. M. and Corfuf, F., Neoarchean greenstone volcanism and continental growth, Dharwar craton, southern India: constraints from SIMS U–Pb zircon geochronology and Nd isotopes. *Precambrian Res*., 2013, **227**, 55–76.
11. Ramarao, Ch., Chetty, T. R. K., Lingaiah, A. and Babu Rao, V., Delineation of a greenstone belt using aeromagnetic, Landsat and photogeology – a case study from the South Indian Shield. *Geoexploration*, 1991, **28**, 121–137.
12. Rama Rao, Ch., Bhaskara Rao, D. S. and Atchuta Rao, D., Delineation of possible extension of a schist belt complex in the southwestern part of the Cuddapah basin from regional aeromagnetic anomaly map – a directional spectral approach. *J. Indian Geophys. Union*, 1993, 99–103.
13. Rama Rao, J. V., Balakrishna, B., Murty, N. V. S., Ajaykumar, P., Ramakrishna Rao, M. V., Acharya, R. S. and Sankaram, S. P., A comprehensive view from geophysical signatures over Chitradurga schist belt, Karnataka. *J. Geol. Soc. India*, 2015, **86**, 489–499.
14. Rao, C. R., Babu, B. B. and Kishore, R. K., Depth estimation to the basement of Vibhutigadda and Talluru formations in the southeast fringe of Sandur schist belt from aeromagnetics. *J. Geol. Soc. India*, 2007, **69**, 732.
15. Satish Kumar, K., Srinivas, K. N. S. S. S., Pradeep Kumar, V., Prabhakara Prasad, P. and Seshunarayana, T., Magnetic mapping of banded iron formation of Sandur schist belt, Dharwar Craton, India. *J. Geol. Soc. India*, 2018, **91**, 174–180.
16. Beard, L. S., Detection and identification of north–south trending magnetic structures near the magnetic equator. *Geophys. Prospect*, 2000, **48**, 745–761.
17. Nabighian, M. N., The analytic signal of two-dimensional magnetic bodies with polygonal cross-section: its properties and use for automated anomaly interpretation. *Geophysics*, 1972, **37**, 507–517.
18. Nabighian, M. N., Additional comments on the analytic signal of two dimensional magnetic bodies with polygonal cross-section. *Geophysics*, 1974, **39**, 85–92.
19. Roest, W. R., Dañobeitia, J. J., Verhoef, J. and Collette, B. J., Magnetic anomalies in the canary basin and the Mesozoic evolution of the central North Atlantic *Mar. Geophys. Res.*, 1992, **14**, 1–24.
20. MacLeod, I. N., Jones, K. and Dai, T. F., 3D analytical signal in the interpretation of total magnetic field data at low magnetic latitudes. *Exp. Geophys*., 1993, **24**, 679–688.
21. MacLeod, I. N., Vierra, S. and Chaves, A. C., Analytic signal and reduction-to-the-pole in the interpretation of total magnetic field data at low magnetic latitudes. In Proceedings of the Third International Congress of the Brazilian Society of Geophysics. SBGf, Anais, 1992, pp. 830–835.
22. PGW, Program documentation – MAGMOD version 1.4. Magnetic interpretation software library, Paterson, Grant and Watson Ltd, Toronto, Canada, 1982.
23. Marquardt, D., An algorithm for least-squares estimation of nonlinear parameters. *SIAM J. Appl. Math.*, 1963, **11**, 431–441.
24. GEOSOFT OASIS MONTAJ GM-SYS version 7.0. Gravity and magnetic modeling software user guide, Northwest Geophysical Associates, Inc, 2004.
25. Talwani, M., Worzel, J. L. and Landisman, M., Rapid gravity computations for two-dimensional bodies with application to the Mendocino submarine fracture zone. *J. Geophys. Res.*, 1959, **64**, 49–59.
26. Talwani, M. and Heirtzler, J. R., Computation of magnetic anomalies caused by two-dimensional bodies of arbitrary shape. In *Computers in the Mineral Industries*, *Part 1* (eds Parks, G. A.), Stanford Univ. Publ. Geol. Sciences, CA, USA, 1964, vol. 9, pp. 464–480.
27. Won, I. J. and Bevis, M., Computing the gravitational and magnetic anomalies due to a polygon. Algorithms and FORTRAN Subroutines. *Geophysics*, 1987, **52**, 232–238.
28. Shuey, R. T. and Pasqulae, A. S., End corrections in magnetic profile interpretation. *Geophysics*, 1973, **52**, 232–238.
29. Cady, J. W., Calculation of gravity and magnetic anomalies along profiles with end corrections and inverse solutions for density and magnetization. Open-File Report No. 77-463. US Geological Survey, Reston, USA, 1977.
30. Cady, J. W., Calculation of gravity and magnetic anomalies of finite-length right polygonal prisms. *Geophysics*, 1980, **45**, 1507–1512.
31. Manikyamba, C., Kerrich, R., Naqvi, S. M. and Ram Mohan, M., Geochemical systematics tholeiitic basalts from the 2.7 Ga Ramagiri–Hungund composite greenstone belt, Dharwar Craton. *Precambrian Res*., 2004, **134**, 21–39.
32. Lowrie, W., *Fundamental of Geophysics*, Cambridge University Press, UK, 2007, 2nd edn.
33. Reynolds, J. M., *An Introduction to Applied and Environmental Geophysics*, John Wiley, UK, 2011, 2nd edn.
34. Telford, W. M., Geldart, L. P. and Sherief, R. E., *Applied Geophysics*, Cambridge University Press, 1990, 2nd edn.
35. Ghosh, D. B., Sastry, B. B. K., Rao, A. J. and Rahim, A. A., Ore environment and ore genesis in Ramagiri schist belt, Andhra Pradesh, India. *Econ. Geol*., 1970, **65**, 801–814.
36. Ramakrishnan, M. and Sundaravanan, D., Differentiated gabbro granophyre composite sill from Ramagiri Greenstone Belt, Andhra Pradesh. *J. Geol. Soc. India*, 1990, **35**, 367–369.

ACKNOWLEDGEMENTS. We thank the Director, CSIR–National Geophysical Research Institute (NGRI), for permission to publish this work (contribution number: NGRI/Lib/2019/Pub-21).

Received 5 April 2019; revised accepted 14 October 2019

doi: 10.18520/cs/v118/i9/1420-1431